Electronic Supplementary Information (ESI):

In situ creating interconnected pores across 3D graphene architectures and their application as high performance electrodes for flow-through deionization capacitors

Hui Wang,[‡] Tingting Yan,[‡] Peiying Liu, Guorong Chen, Liyi Shi, Jianping Zhang, Qingdong Zhong and Dengsong Zhang*

School of Material Science and Engineering, Research Center of Nano Science and Technology, Shanghai University, Shanghai 200444, China.

E-mail: dszhang@shu.edu.cn; Fax: +86 21 66136079.

‡ These authors contributed equally to this work.
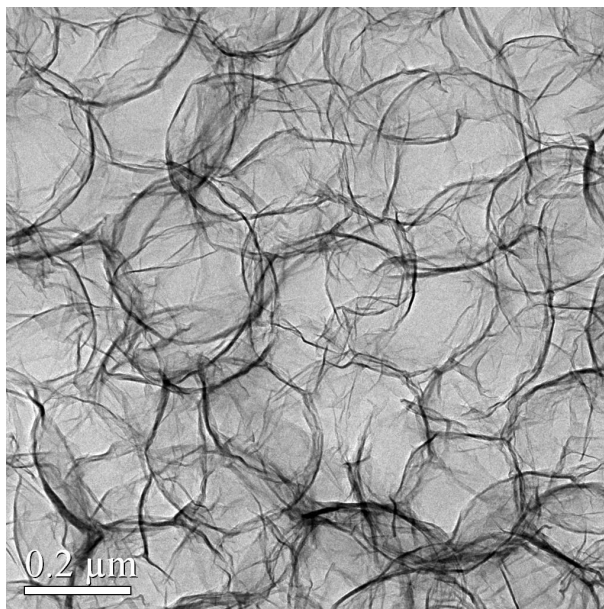
Results and discussion
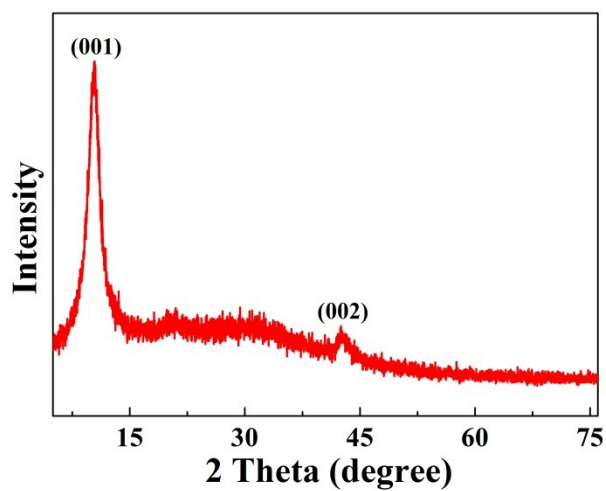

Fig.S1 TEM image of 3DGR.

Fig.S2 XRD pattern of GO.

For GO, only one diffraction peak corresponding to (001) planes can be identified, indicating that the interlayer spacing of GO is larger than that of graphite, because oxygen functional groups were well introduced on the graphite sheets after oxidizing (Fig.S3). Another small wide peak around $2h = 24 \degree$ can also be observed, which is the characteristic (002) peak of residual unoxidized graphite.
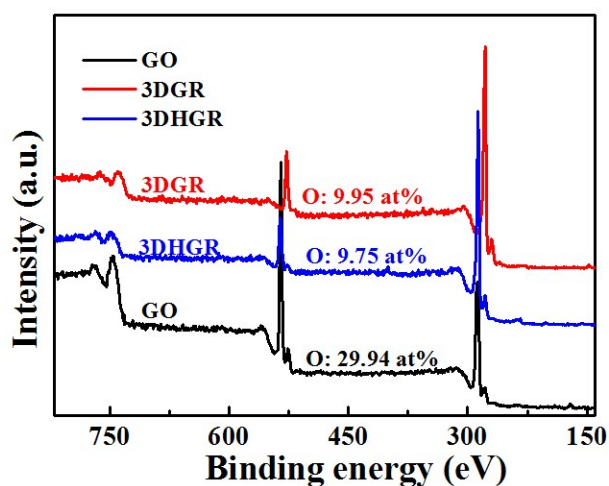
Fig.S3 The XPS spectra of GO, 3DGR and 3DHGR.

The full XPS spectra of GO, 3DGR and 3DHGR are shown in Fig.S3. The oxygen content of GO, 3DGR and 3DHGR is 29.94 at%, 9.95 at% and 9.75 at%. Obviously, the oxygen content of 3DGR and 3DHGR is much lower that of GO, suggesting the effective removal of oxygen functional groups of GO. Furthermore, the oxygen content of 3DGR and 3DHGR is comparable or lower than other graphene-based materials in the previous works.[1-5] Besides, the oxygen content on the surface of 3DGR and 3DHGR is quite close, indicating the similar surface properties of 3DGR and 3DHGR.
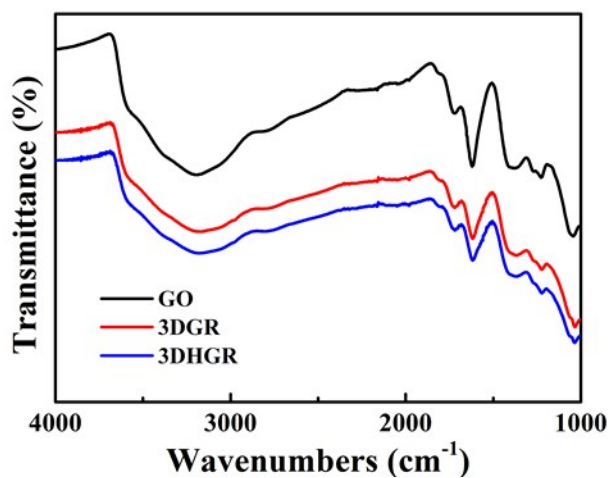
Fig.S4 FTIR spectra of GO, 3DGR and 3DHGR.

The FTIR spectra of GO, 3DGR and 3DHGR are shown in Fig.S4. The presence of intense bands at 1050 cm^{-1}, 1620 and 1720 cm^{-1} are generated by C–O stretching, C=O and COOH vibrations, respectively. The broad band at around 2500-3700 cm^{-1} is for –OH and adsorbed water. After thermal reduction, the intensity of the oxygen functional group is much weaker than that of GO, indicating the reduction of GO.[6, 7] Besides, the intensity of oxygen functional groups between 3DGR and 3DHGR is quite close, which suggests the similar surface properties.
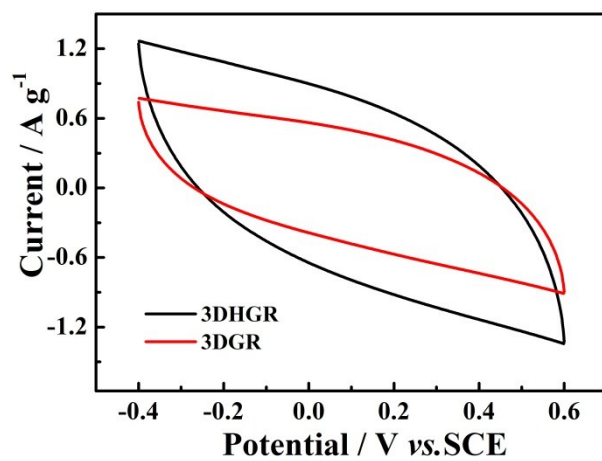
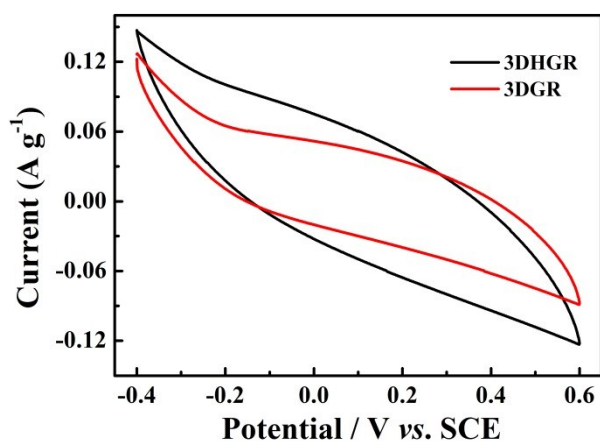Fig.S5 CV curves of the 3DHGR and 3DGR electrodes in a 0.5 M NaCl solution at a scan rate of 10 mV s^{-1}.

Fig.S6 The CV curves of 3DHGR and 3DGR electrodes at 1 mVs^{-1} in a 0.009 M (500 ppm) NaCl solution.

The CV curves of 3DHGR and 3DGR electrodes in a much lower NaCl solution (500 ppm) is shown in Fig.S6. The scan rate is 1.0 mVs^{-1}. The CV curves present a leaf-like shape instead of rectangular-like structure due to the much lower ionic strength in a NaCl solution with low concentration. It should be noted that the CV curve area of 3DHGR electrode is larger than that of 3DGR, indicating the higher specific capacitance of 3DHGR electrodes. Therefore, 3DHGR with hierarchical pore structure (micro-, meso- and macropores) is beneficial to ion adsorption.

Table S1 Comparison of the electrosorption performance among different carbon-based electrodes reported in the literature.

Electrode material	Applied voltage (V)	Initial concentration (mg L^{-1})	Deionization Time (min)	SAC (mg g^{-1})	Ref.
AC	1.2	500	180	4.3	[8]
PCS	1.6	500	40	5.8	[9]
CNTs	1.2	500	40	2.8	[9]
CNFs	1.6	95	150	4.6	[10]
GNFs	2.0	25	40	1.4	[11]
GR	2.0	~50	60	5.0	[12]
PG	1.8	~50	40	3.8	[6]
N-GR	1.8	~50	40	4.8	[13]
S-GR	2.0	250	100	8.6	[14]
GR-AC	1.2	400	30	7.2	[15]
GR-AC	1.2	500	60	2.9	[16]
GR-CNT	2.0	29	60	1.4	[17]
N-GR/CNF	1.2	500	40	11.5	[18]
3DGR	1.2	500	60	6.2	This work
3DHGR	1.2	300	60	11.9	This work
3DHGR	1.2	500	40	13	This work
3DHGR	1.2	500	60	14.7	This work

References

1. X. T. Xu, Y. Liu, T. Lu, Z. Sun, D. H. C. Chua and L. K. Pan, *Journal of Materials Chemistry A*, 2015, **3**, 13418-13425.
2. S. D. Perera, R. G. Mariano, N. Nijem, Y. Chabal, J. P. Ferraris and K. J. Balkus, *J Power Sources*, 2012, **215**, 1-10.
3. S. Dubin, *ACS Nano*, 2010, **4**, 3845–3852.
4. C. M. Chen, J. Q. Huang, Q. Zhang, W. Z. Gong, Q. H. Yang, M. Z. Wang and Y. G. Yang, *Carbon*, 2012, **50**, 659-667.
5. V. H. Pham, H. D. Pham, T. T. Dang, S. H. Hur, E. J. Kim, B. S. Kong, S. Kim and J. S. Chung, *J Mater Chem*, 2012, **22**, 10530-10536.
6. S. Thakur and N. Karak, *Carbon*, 2012, **50**, 5331-5339.
7. A. Ambrosi, C. K. Chua, A. Bonanni and M. Pumera, *Chem Mater*, 2012, **24**, 2292-2298.
8. Z. Chen, C. Song, X. Sun, H. Guo and G. Zhu, *Desalination*, 2011, **267**, 239-243.
9. Y. Liu, L. K. Pan, T. Q. Chen, X. T. Xu, T. Lu, Z. Sun and D. H. C. Chua, *Electrochim Acta*, 2015, **151**, 489-496.
10. G. Wang, C. Pan, L. P. Wang, Q.g Dong, C. Yu, Z. B. Zhao and J. S. Qiu, *Electrochim Acta*, 2012, **69** 65-70.
11. H. B. Li, L. D. Zou, L. K. Pan and Z. Sun, *Environ Sci Technol*, 2010, **44**, 8692-8697.
12. Z. Y. Yang, L. J. Jin, G. Q. Lu, Q. Q. Xiao, Y. X. Zhang, L. Jing, X. X. Zhang, Y. M. Yan and K. N. Sun, *Adv Funct Mater*, 2014, **24**, 3917-3925.
13. X. T. Xu, L. K. Pan, Y. Liu, T. Lu and Z. Sun, *J Colloid Interf Sci*, 2015, **445**, 143-150.
14. B. P. Jia and L. D. Zou, *Carbon*, 2012, **50**, 2315-2321.
15. Q. Dong, G. Wang, B. Q. Qian, C. Hu, Y. W. Wang and J. S. Qiu, *Electrochim Acta*, 2014, **137**, 388-394.
16. H. B. Li, L. K. Pan, C. Y. Nie, Y. Liu and Z. Sun, *J Mater Chem*, 2012, **22**, 15556-155561.
17. H. Li, S. Liang, J. Li and L. He, *J Mater Chem A*, 2013, **1**, 6335-6341.
18. Y. Liu, X. T. Xu, T. Lu, Z. Sun, D. H. C. Chua and L. K. Pan, *Rsc Advances*, 2015, **5**, 34117-34124.